

Kinematics of H₂O masers in high-mass star forming regions

C. Goddi^{1,2}, L. Moscadelli¹, W. Alef³, A. Tarchi^{1,4}, J. Brand⁴, and M. Pani²

¹ INAF, Osservatorio Astronomico di Cagliari, Loc. Poggio dei Pini, Str. 54, 09012 Capoterra (CA), Italy

² Dipartimento di Fisica, Università degli Studi di Cagliari, S.P. Monserrato-Sestu Km 0.7, I-09042 Cagliari, Italy

³ Max-Planck-Institut für Radioastronomie, Auf dem Hügel 69, D-53121 Bonn, Germany

⁴ Istituto di Radioastronomia CNR, Via Gobetti 101, 40129 Bologna, Italy

Received “date” / Accepted “date”

Abstract.

We have conducted multi-epoch EVN observations of the 22.2 GHz water masers towards four high-mass star forming regions (Sh 2-255 IR, IRAS 23139+5939, WB89-234, and OMC2). The (three) observing epochs span a time range of 6 months. In each region, the H₂O maser emission likely originates close (within a few hundreds of AU) to a forming high-mass YSO. Several maser features (~ 10) have been detected for each source and, for those features persistent over the three epochs, proper motions have been derived. The amplitudes of the proper motions are found to be larger than the range of variation of the line-of-sight velocities and in each of the observed sources the proper motion orientation seems to indicate an expansion motion. The gas kinematics traced by the 22.2 GHz H₂O masers is compatible with the shock-excited nature of water maser emission.

Three different kinematic models (a spherical expanding shell, a Keplerian rotating disk, and a conical outflow) were fitted to the 3-dimensional velocity field of the detected maser features. The results of these fits, together with the comparison of the VLBI maps with the highest-resolution images of the sources in several thermal tracers, suggest that the water maser features are most likely tracing the inner portion of the molecular outflows detected at much larger-scales.

Key words. masers – stars: formation – ISM: kinematics and dynamics – Radio lines: ISM

1. Introduction

Comparing the present state of knowledge of the formation process of high-mass ($M \geq 10 M_{\odot}$) and low-mass stars, one can appreciate how little is known about high-mass star formation. High-angular (~ 1 arcsec) resolution observations over an extended range of wavelengths (from centimeter to Near-Infrared (NIR)) have made it possible to recognize different evolutionary classes of low-mass pre-main-sequence stars (from Class 0 to Class II; e.g. André et al. 1993; hereafter AWB). On the other hand, for the high-mass counterpart, only a tentative protostellar evolutionary scheme presently exists, and it is often hard to distinguish between protostars and young Zero Age Main Sequence (ZAMS) stars. This lack of knowledge is a direct consequence of difficulties in observing the earliest evolutionary phases of massive Young Stellar Objects (YSOs), because high-mass stars are rare, form on much shorter timescales ($\sim 10^5$ yr) than those required for low-mass formation, and the sites of massive star formation are found at much larger distances (typically several kilo-

parsecs), requiring high-angular resolution observations. High-mass stars also spend all of their pre-main sequence phase deeply embedded in their natal molecular cloud (in fact they arrive on the main sequence while still accreting matter), suffering high extinction which prevents their detection at optical and (quite often) NIR wavelengths.

A powerful diagnostic tool to investigate the first stages of the formation of massive stars is provided by Very Long Baseline Interferometry (VLBI) observations of the maser transitions of several molecular species, such as OH, H₂O, CH₃OH, observed in the proximity (within a distance ≤ 100 AU) of the high-mass (proto-)stars. In particular, for fast-moving 22.2 GHz water masers, multi-epoch VLBI observations, reaching angular resolutions of ~ 1 mas (corresponding to ~ 1 AU at a distance of 1 kpc), allow accurate proper motions to be determined with time baselines as short as a few months. The measured tangential velocities, combined with the radial velocities derived via the Doppler effect, permit to obtain the 3-dimensional velocity distribution of the maser gas. This technique is presently the only one that has the potential to derive the gas kinematics in the close proximity (few AU) of the (proto-)star.

Table 1: Description of the observed sources

Source name	Coordinates (1950)		V_{cloud} (km s $^{-1}$)	Distance (pc)	L_{bol} ($10^3 L_{\odot}$)
	RA (h m s)	DEC ($^{\circ} \text{ } '$ '')			
Sh 2-255 IR	06 09 58.60	+18 00 13.0	7.2 ^a	2500 ^b	9.0 ^c
IRAS 23139+5939	23 13 58.91	+59 39 06.0	-44 ^d	4800 ^d	25 ^d
WB89-234	23 00 24.1	+56 41 42.2	-53.4 ^e	5800 ^e	10 ^e
OMC2	05 32 59.9	-05 11 26.8	12 ^f	480	1.5 ^g

Note.— ^a Miralles et al. 1997; ^b Evans et al. 1977; ^c Mezger et al. 1988; ^d Sridharan et al. 2002; ^e Brand & Wouterloot 1998; ^f Aso et al. 2000; ^g Rengarajan & Ho 1996.

Recent VLBI observations have shown that 22.2 GHz water masers are preferentially associated with collimated flows of gas (jets) found at the base of larger-scale molecular outflows (IRAS 05413-0104, Claussen et al. 1998; IRAS 20126+4104, Moscadelli et al. 2000; W3 IRS 5, Imai et al. 2000; W75N-VLA1, Torrelles et al. 2003). In a few cases, linear clusters (size \sim 10-100 AU) of maser features have been interpreted in terms of accretion disks (e.g., NGC 2071 IRS 1 and IRS 3, Seth et al. 2002; AFGL 5142, Goddi et al. 2004, hereafter Paper I).

Accretion disks were proposed originally to explain Very Large Array (VLA) observations of water masers (e.g., Cepheus A, Torrelles et al. 1996; W75N-VLA2, Torrelles et al. 1997). Successive Very Long Baseline Array (VLBA) observations (with a gain in resolution of $\sim 10^3$) by Torrelles et al. (2001, 2003), however, have revealed that the water maser features closer to the YSOs are distributed along perfectly circular arcs (radius 62 AU for Cepheus A R5, 160 AU for W75N-VLA2), which are also expanding (with velocities of 10 km s $^{-1}$ for Cepheus A, 28 km s $^{-1}$ for W75N-VLA2). The authors interpret these structures as being due to a spherical ejection of material from a YSO located at the center of the maser circle, demonstrating that clusters of water maser features close (within hundreds of AU) to the YSO may participate in expanding motions driven by a wide-angle wind, rather than be subject to rotating motions.

Measurements of the maser feature proper motions are essential to distinguish between the different kinematic scenarios, allowing to clarify whether the maser clusters are expanding from the YSO (supporting the collimated or wide-angle wind interpretation) or rather rotating and contracting (in agreement with the disk model). So far, only a relatively small number (\approx 10) of intermediate and/or high-mass YSOs have been studied with multi-epoch VLBI observations of the 22.2 GHz water masers.

Torrelles et al. (2003) proposed also that different kinematic structures (spherical shells vs. collimated flows) traced by the water masers represent different evolutionary stages of the YSO. In this view, in the earliest evolutionary phases YSOs would emit wide-angle winds, whilst during later phases the material ejection would become more collimated. Therefore, these recent observational re-

sults open up the interesting perspective of using the 22.2 GHz water masers to derive information on the evolutionary stage of high-mass YSOs.

In Paper I we presented the results of an European VLBI Network (EVN) multi-epoch study of the 22.2 GHz water masers towards the high-mass star forming region (SFR) AFGL 5142. In the following, we report the results of water maser EVN observations of 4 additional high-mass YSO-candidates (Sh 2-255 IR, IRAS 23139+5939, WB89-234, OMC2).

Section 2 of this paper describes our multi-epoch EVN observations and gives technical details of the data analysis. Section 3 presents the observational results. In Section 4, we investigate plausible kinematic models for interpreting the measured positions and velocities of the maser features, explore the physical environment of the observed sources as implied by the kinematic considerations, and discuss the way of deriving an evolutionary pattern for the studied YSOs. Finally, conclusions are drawn in Section 5.

2. Observations and data reduction

The four high-mass YSOs were observed in the $6_{16} - 5_{23}$ H₂O maser line (rest frequency 22235.080 MHz) using the EVN at three epochs (June, September, and November, 1997). A description of the most relevant properties (i.e., source name, coordinates, velocity of the ambient medium, distance and bolometric luminosity) of each source is given in Table 1.

An extensive description of the observations and of the data reduction process has already been provided in Paper I. Hence, here we describe only the observational parameters, summarized in Table 2, peculiar to the individual sources. For each epoch, we used as phase-reference the peak intensity channel, which exhibits in all cases a simple spatial structure consisting of a single, unresolved spot. Due to the high water maser variability, the peak maser emission may vary in velocity (and position) from epoch to epoch. In particular, for the source Sh 2-255 IR the phase reference component of the third observing epoch differs from the one used at the previous two epochs (see Table 2). However, the maser components selected as phase refer-

ence were present at all the observing epochs, allowing us to confidently align maps of different epochs.

For all the four sources and the three observing epochs, we produced (naturally weighted) maps extended over a sky area of $(\Delta\alpha \cos\delta \times \Delta\delta) 2'' \times 2''$. The CLEAN beam was an elliptical gaussian, with FWHM size and position angle varying with the epoch (see Col. 5 of Table 2). The RMS noise level on the channel maps, σ , (reported in Col. 6) varies significantly, being close to the theoretical thermal value for channels where no signal is detected and increasing up to one (or even two) orders of magnitude for channels with the strongest components.

Every channel map has been searched for emission above a conservative detection threshold, taken equal to the absolute value of the minimum in the map corresponding to a multiple of the rms noise by a factor in the range 5–10. The detected maser spots have been fitted with two-dimensional elliptical Gaussians, determining position, flux density, and FWHM size of the emission.

Following Paper I, we define a “maser feature” as a group of maser spots detected in at least three contiguous channels, with a position shift of the intensity peak from channel to channel smaller than the FWHM size.

3. Observational results

In this section we present the VLBI maps of the observed water maser sources. From a comparison between these VLBI maps and those, at lower resolution, available in the literature, we can obtain further insights on the nature of the sources responsible for the water maser excitation. VLA maps of the 22 GHz water maser emission were available for all the sources.

We have tentatively derived an absolute position for the EVN 22.2 GHz maser maps when the VLA and EVN strongest features were found to emit at the same LSR velocity, and under the assumption that the most intense maser emission emerges always from the same position. In doing so, the derived absolute position of the VLBI reference feature has an error equal to (or greater than) the VLA positional uncertainty.

Table 3 reports the parameters of the identified water maser features. The procedure to derive (relative) positions, proper motions, and associated errors is described in detail in Paper I. In particular, we note that for each source the feature selected to refer positions and velocities to, is chosen using the criterion of increasing the amplitude of the relative proper motions, hence maximizing their SNR. The selected reference maser feature may have its own (absolute) proper motion, resulting in arbitrary offsets in the proper motions for the other features.

3.1. Sh 2-255 IR

The high-mass star forming complex Sh 2-255 IR, at a distance of 2.5 kpc from the Sun (Evans et al. 1977), is located between the two HII regions S255 and S257. VLA observations at 5 GHz (2.''6 beam) detected three

compact HII regions associated with Sh 2-255 IR (Sh 2-255-2a, -255-2b and -255-2c), each one corresponding to a ZAMS star of spectral type B1 (Snell & Bally 1986). Successively, higher-resolution VLA observations at 15 GHz (beam $\approx 0.''5$) have revealed a continuum emission (flux density ≈ 1.97 mJy) coincident with Sh 2-255-2c (Rengarajan & Ho 1996).

Sh 2-255 IR was imaged by Miralles et al. (1997) at NIR and mm wavelengths, revealing a cluster of 50 NIR sources, associated with Herbig Haro-like objects, IR H₂ jets and molecular outflows. The reddest source in the region, NIR 3, coincident with the radio source Sh 2-255-2c, is interpreted in terms of a YSO powering an infrared H₂ jet (aligned at P.A. $\approx 67^\circ$) and a CO compact outflow (size $\leq 1'$), approximately oriented parallel to the infrared-jet axis (Miralles et al. 1997; see their Fig. 9). High-resolution (beam $\approx 1.''5$) NIR observations of the H₂ 2.122 μ m and of the Br γ hydrogen recombination lines by Howard et al. (1997) confirm the presence of an ionized jet (shown in the upper panel of Fig. 1), likely originating from IRS1 (NIR 3 in the notation of Miralles et al. 1997), a YSO candidate detected both at near- and mid-infrared wavelengths.

22.2 GHz water maser VLA observations (unpublished data kindly provided by R. Cesaroni) at two epochs (March 1990; August 1991) reveal three emission centers over a region of a few arcseconds (see middle panel of Fig. 1), with the strongest maser feature (≈ 30 Jy) found to be coincident in position with Sh 2-255-2c.

The lower panel of Fig. 1 shows the positions and velocities of the 22.2 GHz maser features as derived by our multi-epoch EVN observations. Maser features show an elongated spatial distribution of size ≈ 700 AU whose major axis is oriented approximately parallel to the ionized jet axis observed at arcsec-scale using the Br γ and H₂ 2.12 μ m lines. The line-of-sight velocity dispersion in the molecular outflow agrees well with the LSR velocity dispersion of VLBI maser features. All the measured *relative* proper motions are approximately perpendicular to the jet axis, and have amplitudes (in the range 10–40 km s $^{-1}$) large compared to the spread of radial velocities (≈ 7 km s $^{-1}$).

3.2. IRAS 23139+5939

A multi-wavelength study of IRAS 23139+5939 (at a distance of ≈ 4.8 kpc) conducted by Sridharan et al. (2002) and Beuther et al. (2002b) have revealed a mid-infrared source (positional accuracy $\approx 5''$), coincident in position with a Plateau de Bure (PdB) 1.2 mm continuum source (flux density ≈ 2.3 Jy, for an observing beam $\approx 5''$) and with a faint 3.6 cm continuum source detected at two different epochs with the VLA (1992, 0.6 mJy flux density with a 0.''3 beam, Tofani et al. 1995; 1998, 1.4 mJy flux density with a 0.''7 beam, Sridharan et al. 2002). The cm-source has been interpreted in terms of (optically thin) free-free emission but no spectral index information was provided to support this interpretation.

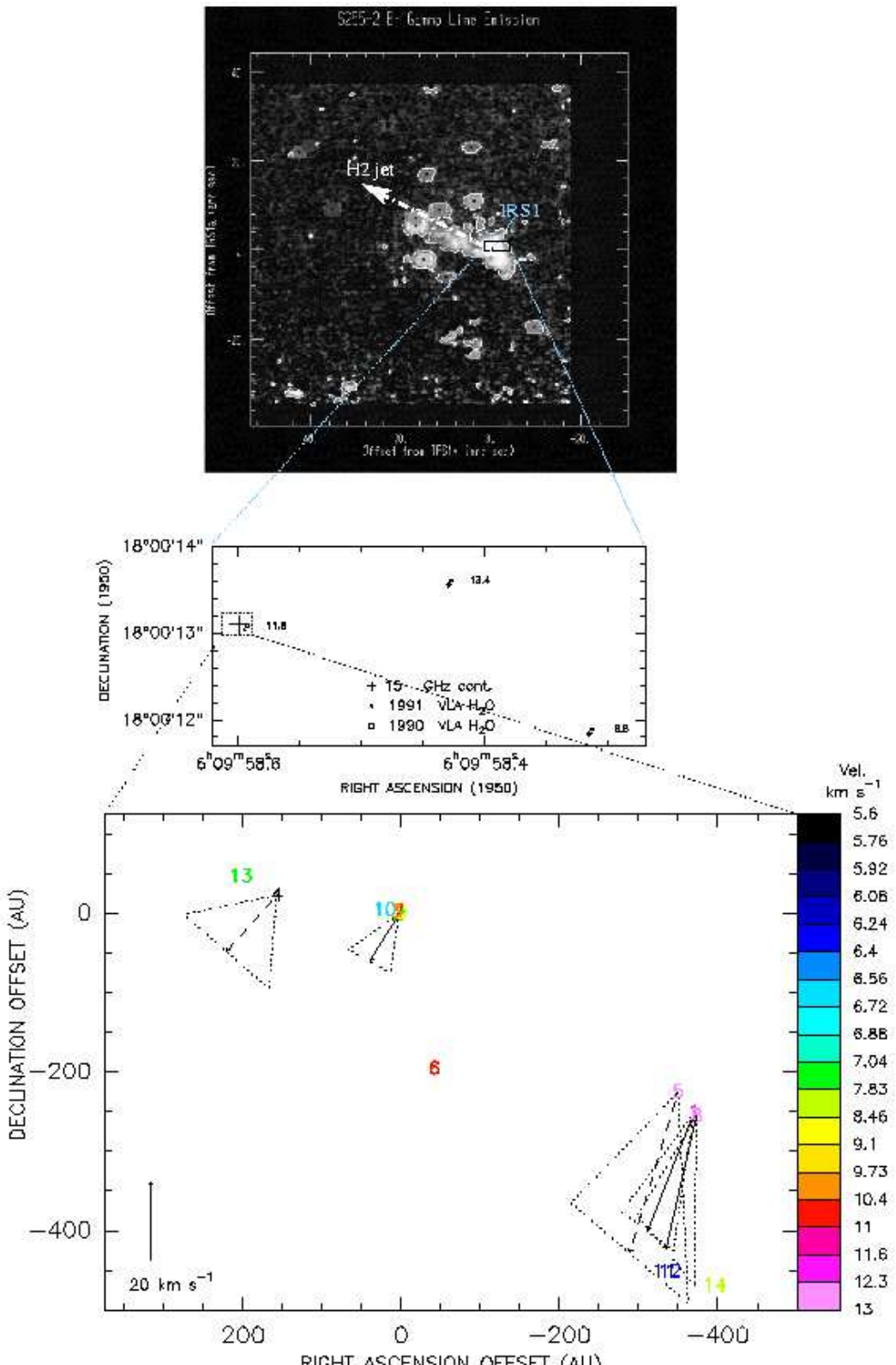


Fig. 1. Sh 2-255 IR. (*Upper panel*) $\text{Br}\gamma$ line minus continuum emission (Howard et al. 1997); the white-dashed arrow indicates the proposed orientation of the jet observed also in the H_2 2.12 μm emission (P.A. $\approx 67^\circ$); the origin of the map coincides with IRS1 at $\alpha(1950) = 06^h 09^m 58^s.6$, $\delta(1950) = 18^\circ 00' 13''$. (*Middle panel*) Positions and the LSR velocities of the 22.2 GHz H_2O maser features detected with the VLA in 1990 (*open squares*) and 1991 (*filled dots*) by R. Cesaroni (priv. com.); the cross indicates the positional uncertainty of the VLA 15 GHz continuum source (Rengarajan & Ho 1996). (*Bottom panel*) VLBI 22 GHz water maser features, identified with the label number given in Col. 2 of Table 3. Different colours are used to distinguish the line-of-sight velocities of the features, according to the colour-velocity conversion code shown on the right-hand side of the panel. The arrows indicate the measured proper motions (whose amplitude scale is given at the bottom of the panel), with dashed lines used in case of features detected at only two epochs; the dotted triangles drawn around the arrows represent the orientation uncertainty of the proper motions; dotted lines without error triangles are finally used in the case that the signal-to-noise ratio of

Table 2: Summary of water maser observations

Source	Epoch	P. R. V_{LSR} (km s $^{-1}$)	P. R. intensity (Jy beam $^{-1}$)	Beam size (mas)	RMS noise (mJy beam $^{-1}$)
Sh 2-255 IR	Jun 97	11.6	41.8	1.1×1.0 pa= 83.5°	100-300
	Sep 97	11.8	78.5	2.8×1.2 pa= 50.6°	50-600
	Nov 97	7.6	20.5	1.4×1.0 pa= 86.5°	20-100
IRAS 23139+5939	Jun 97	-53.2	38.6	1.6×1.4 pa= -81.6°	40-500
	Sep 97	-53.3	247.0	2.3×1.6 pa= -41.4°	40-4000
	Nov 97	-53.1	240.0	1.5×1.3 pa= 87.1°	20-2000
WB89-234	Jun 97	-51.1	15.0	1.5×0.7 pa= 42.1°	100-300
	Sep 97	-51.1	17.8	1.4×0.9 pa= -61.9°	200-300
	Nov 97	-51.1	32.4	1.1×0.9 pa= -57.8°	100-300
OMC2	Jun 97	18.0	10.2	2.4×1.6 pa= -38.5°	30-200
	Sep 97	18.0	70.0	2.9×1.4 pa= 43.9°	50-600
	Nov 97	18.0	31.3	2.3×1.1 pa= 54.2°	100-900

Note.— Cols. 3 and 4 give the LSR velocity and the peak intensity of the maser component selected as phase reference.

Nevertheless, these observations strongly suggest the presence of a massive YSO in this region. Its bolometric luminosity, $\approx 2.5 \times 10^4 L_{\odot}$ (Sridharan et al. 2002), would correspond to a ZAMS star of spectral type B0 (Panagia 1973). Unfortunately, the low angular resolutions of the previously listed observations do not allow to establish whether the cm to infrared wavelength emission is powered by a single YSO or is the cumulative result of several distinct sources.

A CO outflow is detected towards IRAS 23139+5939 (Wouterloot et al. 1989; Beuther et al. 2002b), nearly oriented along the line-of-sight and not spatially resolved at single-dish angular resolutions (beam $\approx 11''$) (Fig. 2, upper panel).

The 22.2 GHz water masers were observed using the VLA by Tofani et al. (1995) (0''.1 beam) and Beuther et al. (2002c) (0''.4 beam). Tofani et al. (1995) detected 4 maser features distributed at the center of the molecular outflow (with line-of-sight velocities in agreement with the blue-shifted lobe): three of these are clustered around the 8.4 GHz continuum source, while the fourth is offset from it by 5'' (Fig. 2, middle panel). Beuther et al. (2002c) detected only the maser features associated to the radio continuum source but a precise correspondence between the features at the two VLA epochs is impossible because of the different accuracy in absolute positions (0''.1, Tofani et al. 1995; 1'', Beuther et al. 2002c).

Fig. 2 (lower panel) shows positions and velocities of the 22.2 GHz maser features as derived from our multi-epoch EVN observations. Most of the 22.2 GHz emission emerges from a cluster of maser features whose diameter is ≈ 200 AU, adopting a kinematic distance of 5 kpc. Most of the VLBI features have line-of-sight velocities

blue-shifted with respect to the quiescent gas velocity (≈ -44 km s $^{-1}$) and distributed over the whole velocity range of the blue-shifted lobe of the CO molecular outflow, $\Delta v = (-59, -47)$ km s $^{-1}$ (Beuther et al. 2002b). Although only a small number of proper motions is derived, they are suggestive of a general expansion motion with (relative) velocities of tens of km s $^{-1}$ (see Sect. 4).

3.3. WB89-234

WB89-234 (at a distance of 5.8 kpc) was first detected by Wouterloot & Brand (1989) during a survey of CO emission towards IRAS sources in SFRs and subsequently studied in detail by Brand & Wouterloot (1998). Fig. 3 (upper panels) shows that the H₂O maser (whose absolute position is derived from VLA observations; Brand & Wouterloot, unpublished) is found at the center of a CO bipolar outflow and coincides with a NIR source (imaged in J, H, K bands, and in the H₂ 2.12 μ m line), which probably identifies the embedded exciting YSO. The associated water maser has been regularly monitored with the Medicina 32-m radiotelescope during the last ten years (from 1994 to 2004), revealing a velocity range of emission roughly constant between -60 and -50 km s $^{-1}$ (within the velocity range of the CO outflow), with the strongest component usually at ≈ -51 km s $^{-1}$.

The 22.2 GHz maser features detected in our EVN maps (Fig. 3, bottom panel) present a line-of-sight velocity dispersion consistent with the Medicina observations (with the intensity-peak at -51.1 km s $^{-1}$) and are distributed across an area of diameter ≈ 900 AU. The maser spatial distribution shows no preferential direction of elongation. All the measured *relative* proper motions have similar northwest-southeast orientation (close to the direction

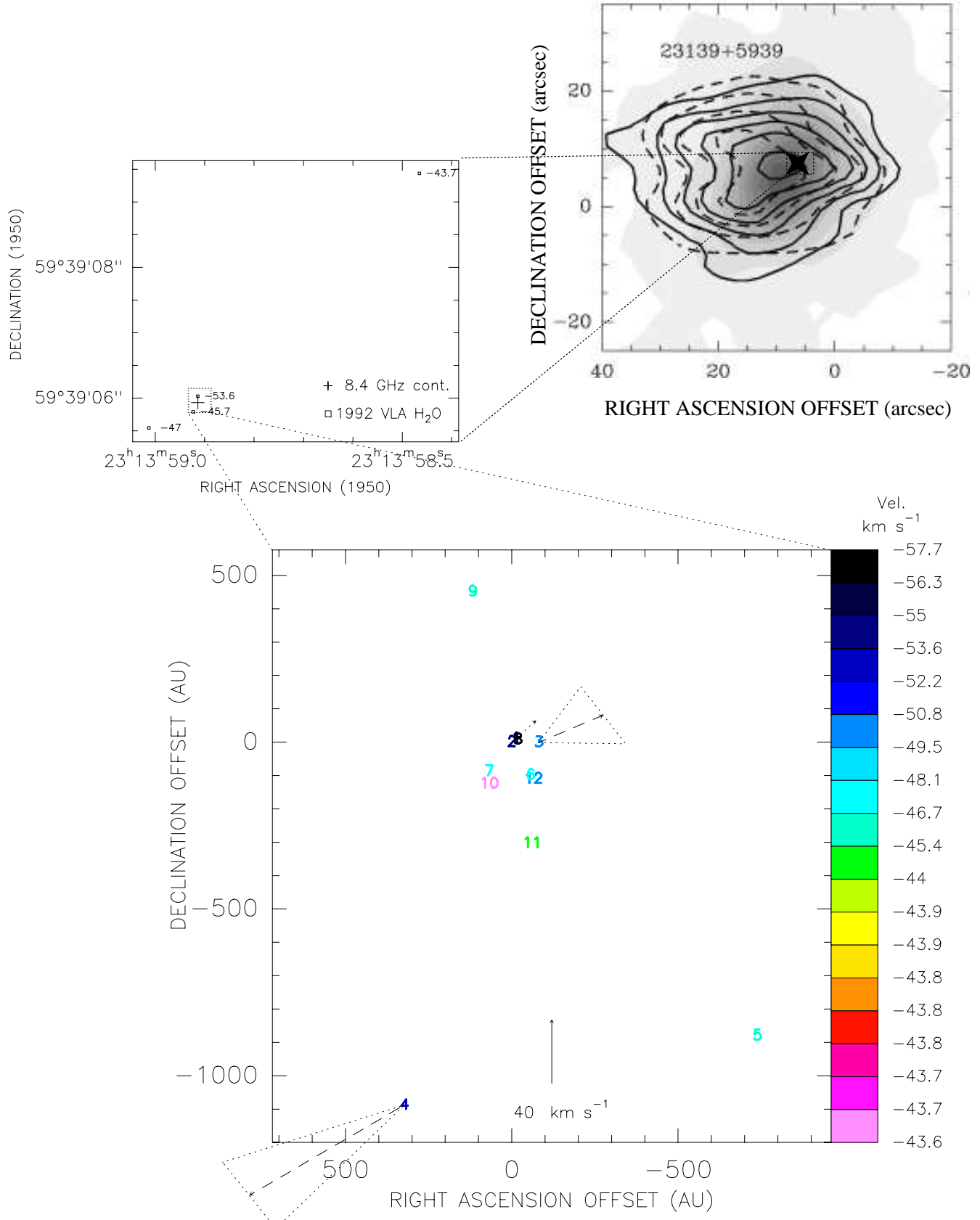


Fig. 2. IRAS 23139+5939. (Upper panel) Blue lobe (solid lines) and red lobe (dashed lines) of CO 2-1 emission mapped with the PdB by Beuther et al. (2002b), overlapped with the PdB 1.2 mm continuum emission (grey scale); the axes show offsets in arcsec from the absolute IRAS-position: $\alpha(1950)=23^h13^m58^s.016$, $\delta(1950)=59^{\circ}38'59.''890$ (Sridharan et al. 2002); the filled star indicates the position of the infrared source. (Middle panel) Positions (open squares) and the LSR velocities of 22.2 GHz H_2O maser features detected with the VLA in 1992 by Tofani et al. (1995); the cross indicates the positional uncertainty of the 8.4 GHz continuum source. (Bottom panel) VLBI map of the 22.2 GHz water maser features (see the caption of Fig. 1); the axes show offsets in AU from the absolute position: $\alpha(1950)=23^h13^m58^s.914$, $\delta(1950)=59^{\circ}39'06.''03$, corresponding to the feature with label number “2”.

Table 3: Maser feature parameters

Source name	Feature	V_{LSR} (km s $^{-1}$)	F_{int} (Jy)	$\Delta\alpha$ (mas)	$\Delta\delta$ (mas)	V_x (km s $^{-1}$)	V_y (km s $^{-1}$)	V_{mod} (km s $^{-1}$)
Sh 2-255 IR	1	11.6	51.9	-147.8 (0.1)	-100.69 (0.09)	8 (7)	-30 (5)	31 (5)
	2	7.3	24.7	1.4 (0.1)	-0.71 (0.05)	5 (6)	-11 (3)	12 (4)
	3	9.9	2.6	2.77 (0.08)	0.39 (0.05)			
	4	5.6	5.0	63.1 (0.1)	9.09 (0.05)	7 (11) [†]	-14 (9)	16 (9)
	5	12.9	2.4	-140.0 (0.2)	-90.1 (0.2)	14 (15)	-41 (12)	43 (12)
	6	10.5	2.5	-16.7 (0.2)	-78.4 (0.2)			
	7	10.7	2.4	1.5 (0.2)	0.8 (0.2)			
	8	12.5	11.5	-149.2 (0.2)	-102.2 (0.3)	5 (7)	-35 (8)	-35 (8)
	9	9.1	13.9	0.0 (0.2)	0.0 (0.07)	0	0	0
	10	6.7	4.9	8.5 (0.2)	1.6 (0.2)			
	11	5.8	0.6	-132.8 (0.2)	-181.0 (0.2)			
	12	6.4	4.0	-135.6 (0.1)	-180.75 (0.05)			
	13	7.1	2.5	81.3 (0.1)	18.40 (0.05)			
	14	8.5	2.7	-158.3 (0.1)	-187.61 (0.05)			
IRAS 23139+5939	1	-53.2	199.6	-2.81 (0.08)	2.45 (0.06)	-13 (15)	11 (9)	17 (12)
	2	-54.7	7.1	0.00 (0.05)	0.0 (0.05)	0	0	0
	3	-50.5	4.6	-16.82 (0.09)	-0.24 (0.07)	-40 (14)	17 (18)	44 (15)
	4	-52.9	4.8	-67.3 (0.1)	-226.6 (0.1)	97 (17)	-57 (21)	112 (18)
	5	-46.6	4.2	-153.78 (0.08)	-183.4 (0.1)			
	6	-46.7	1.2	-11.70 (0.08)	-20.7 (0.1)			
	7	-47.3	0.9	14.2 (0.2)	-18.2 (0.1)			
	8	-57.7	0.7	-3.7 (0.1)	1.6 (0.1)			
	9	-46.6	0.8	24.49 (0.08)	94.0 (0.2)			
WB89-234	1	-51.0	30.4	94.29 (0.06)	18.21 (0.04)	11 (4)	-20 (5)	23 (5)
	2	-54.9	6.6	0.00 (0.08)	0.00 (0.05)	0	0	0
	3	-55.9	4.7	5.35 (0.07)	-15.46 (0.04)	10 (5)	-31 (2)	33 (3)
	4	-50.1	4.6	32.42 (0.07)	9.11 (0.03)	34 (16)	-37 (5)	50 (11)
	5	-57.0	4.0	3.6 (0.3)	-16.41 (0.09)	0.2 (25)	-65 (8)	65 (8)
	6	-56.0	2.1	-12.04 (0.07)	-13.32 (0.03)			
	7	-58.4	1.4	5.4 (0.2)	-17.15 (0.04)			
	8	-55.9	3.8	5.88 (0.06)	20.31 (0.04)			
	9	-52.4	1.6	5.06 (0.07)	18.24 (0.04)			
	10	-53.8	1.5	-1.69 (0.04)	62.94 (0.02)			
	11	-53.7	1.4	-1.19 (0.08)	-9.65 (0.05)			
	12	-60.4	1.6	44.44 (0.03)	13.73 (0.03)			
OMC2	1	17.6	115.5	0.0 (0.1)	0.00 (0.09)	0	0	0
	2	11.9	2.3	172.7 (0.1)	89.29 (0.09)			
	3	8.5	2.3	158.5 (0.1)	75.2 (0.1)	12 (3)	13 (3)	18 (3)

Note.— Col. 1 gives the source name; for each identified feature Col. 2 reports the label number; Cols. 3 and 4 the line-of-sight velocity and the integrated flux density of the highest-intensity channel; Cols. 5 and 6 the (RA and DEC) relative positional offsets (with the associated uncertainties in parentheses); Cols. 7, 8, and 9 the projected components along the RA and DEC axes, and the absolute value of the derived proper motions.

† The italic character is used to indicate tentative values of proper motion components for features observed either at only two epochs or with a very large uncertainty in the direction of motion.

of the molecular outflow), with amplitudes (in the range $20 - 60$ km s $^{-1}$) large compared with the spread of line-of-sight velocities (≈ 10 km s $^{-1}$).

3.4. OMC2

OMC2, located at a distance of about 480 pc, is one of the most active sites of star formation in the solar neighborhood. A cluster of young infrared sources (Jones et al. 1994) and several submillimeter continuum

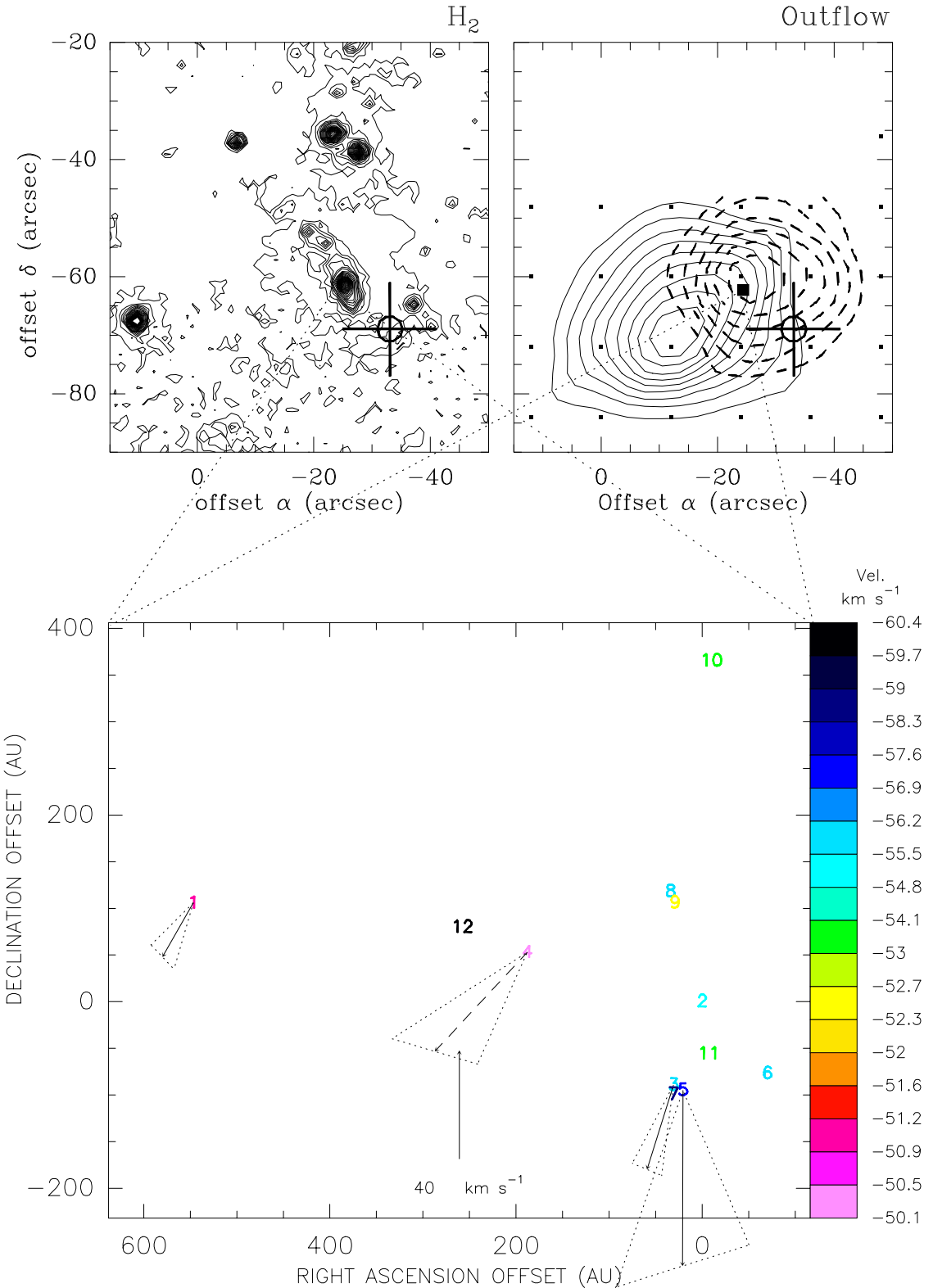


Fig. 3. WB89-234. (Upper panels) TIRGO H_2 2.12 μm image (left); blue (dashed lines) and red (solid lines) lobes of ^{12}CO (1-0) wing emission (Brand & Wouterloot 1998) (right); the big crosses and the filled squares indicate the positional uncertainties of the H_2O maser observed respectively with Effelsberg (Brand & Wouterloot 1998) and the VLA (Brand & Wouterloot, unpublished); the axes show offsets in arcsec from the absolute IRAS-position: $\alpha(1950)=23^{\text{h}}00^{\text{m}}27^{\text{s}}.0$, $\delta(1950)= 56^{\circ}42'45''$. (Bottom panel) VLBI map of the 22.2 GHz water maser features (see the caption of Fig. 1); the origin of the map corresponds to the position of the feature "2", at: $\alpha(1950)=23^{\text{h}}00^{\text{m}}24^{\text{s}}.150$, $\delta(1950)= 56^{\circ}41' 42''.3$.

sources (Mezger et al. 1990; Chini et al. 1997) are found in this region, and 3.6 cm continuum VLA observations ($\approx 8''$ beam) have revealed an unusual concentration of class 0 protostars (Reipurth et al. 1999). One of these radio sources, labeled VLA 11 (Reipurth et al. 1999), is coincident in position with a bright 1.3 mm source, FIR 3 (Mezger et al. 1990), and an infrared source, IRS 4 (detected at several different wavelengths from 1 to 100 μm ; Pendleton et al. 1986), and is also associated with a weak 22 GHz water maser (Genzel & Downes 1979). Besides, VLA 11 is found at the center of a group of bright near-infrared H₂ bow shocks (flow J of Yu et al. 1997) and of a CO and HCO⁺ outflows (Fischer et al. 1985; Aso et al. 2000). The molecular outflows are nearly oriented along the line-of-sight (with the red and the blue lobes spatially overlapped), but unlike the CO outflow, the HCO⁺ outflow is elongated and well correlated with the axis of the H₂ jet (P.A. $\approx 30^\circ$; Fig. 4, upper panel).

High-resolution observations ($\approx 0.''1$ and $0.''5$ beam, respectively), conducted with the VLA at 8.4 GHz (Tofani et al. 1995) and 15 GHz (Rengarajan & Ho 1996), revealed a faint (≈ 2.5 mJy), slightly extended ($0.''8$) continuum source, coincident in position with the sources VLA 11/FIR 3. The radio continuum source is found to be extended along a North-South direction (P.A. 17°) and it is interpreted as optically thin free-free emission from an ionized wind (Rengarajan & Ho 1996), compatible with an intermediate-luminosity ZAMS star (spectral type between B2 and B3).

Using the VLA, Tofani et al. (1995) detected two 22 GHz maser features, placed respectively northward and southward of the 8.4 GHz continuum source, and separated by $\approx 0.''5$ (Fig. 4, middle panel).

Only three maser features have been detected in our EVN maps towards this source and only one “tentative” proper motion has been derived for the feature with label number “3” (Fig. 4, bottom panel). In this case a precise association between the VLA and the VLBI emission is impossible, since no correspondence is found between the line-of-sight velocities of the strongest VLA and VLBI spots. The three features are aligned along a direction similar to the orientation of the measured proper motion. This direction is also similar to the orientation of the large-scale molecular outflow seen in the H₂ and CO emission.

4. Discussion

4.1. Kinematics of the masing gas

In Sect. 3, for each source, we have presented multi-epoch VLBI maps of the water masers and compared them with previous observations in different thermal tracers.

Several concentrations of H₂O maser features are found in each of the observed sources within 1000 AU of the YSO position, which itself is indicated by unresolved radio and/or millimeter continuum sources. Clustered distributions of maser features have been interpreted, depending on the geometrical shape (curved

or linear) and the measured proper motions, in terms of expanding spherical shells (representing wide angle winds) (Torrelles et al. 2001, 2003) and/or jet/disk systems (Seth et al. 2002; Paper I).

There is no clear evidence of spherical structures in the observed water maser distributions. IRAS 23139+5939 shows the most clustered distribution of maser features. Since the spherical geometry might be hidden by projection effects onto the plane of the sky, we constructed a simple kinematic model of spherical expansion, which assumes that the detected maser features belong to the surface of a sphere of given radius and move outward with a velocity increasing with radius. This model was applied to IRAS 23139+5939, but the best fit solution was not physically plausible, since the maser features sampled a very small fraction of the sphere's surface, that moreover was centered well outside the maser region. Hence, we conclude that a spherical expansion model such as that proposed by Torrelles et al. (2001, 2003) for the high-mass YSOs Cepheus A-R5 and W75N-VLA2 does not apply to the distribution of maser features seen towards our sources.

The current theory of star formation foresees that two main kinds of gas motion should be found in the proximity of a forming star: 1) rotation and contraction, under the influence of the gravitational field of the central YSO (resulting in the creation of an accretion disk); 2) expansion, driven by either wide-angle or collimated winds (resulting in the formation of a jet/outflow system). We have tested the expansion vs rotation scenario by fitting the measured positions and velocities of the detected maser features with two simple, mutually exclusive kinematic models: 1) a Keplerian disk; 2) a conical outflow. Since few maser features have been detected and only few accurate proper motions have been measured towards the studied YSOs, we warn that the results obtained from these model fits should be considered only as a test for the physical plausibility of the kinematic structures traced by water masers in the proximity of the massive YSOs, without any claim of conclusiveness.

The free parameters of the Keplerian disk model are: the sky-projected coordinates, α_d (R.A.) and δ_d (Dec), of the YSO (at the disk center); the position angle, P_d , and the inclination angle with the line-of-sight, i_d , of the disk axis; the YSO mass, M_{YSO} . The conical outflow model assumes that the gas moves along the directrices of a conical surface, with a velocity increasing with the distance from the cone vertex following the Hubble law: $\mathbf{v} = a_c \mathbf{r}$, where a_c is the velocity gradient. The parameters of the conical flow are: the sky-projected coordinates, α_c (R.A.) and δ_c (Dec), of the YSO (at the cone vertex); the position angle, P_c , and the inclination angle with the line-of-sight, i_c , of the cone axis; the opening angle of the cone, θ_c ; the velocity gradient a_c .

The parameters of the best fit models are reported in Table 4. The best-fit solution is found minimizing the χ^2 given by the sum of the square differences between the 3-dimensional, relative, model and measured velocities. For WB89-234 and IRAS 23139+5939, a formal solution was

found for both the Keplerian disk and the conical flow model, but only this latter provided a physically reasonable solution (as it will be described in more details in the following). For Sh 2-255 IR a minimum was found only for the conical flow model. No model fit was attempted for OMC2 because of the (too) low number (three) of features detected.

As is evident from Fig. 1 and 4 (lower panels), Sh 2-255 IR and OMC2 show an elongated spatial distribution of water maser features, which are aligned along a direction close to the orientation of the molecular outflows seen at much larger scales. Pure “morphological” considerations might suggest that the maser features are associated with the inner portion of the jet/outflow systems. However, in this case one would also expect the transversal velocities to be mainly directed along the jet/outflow axis. This geometrical condition is observed towards OMC-2, where the single measured (relative) proper motion is approximately oriented along the elongation axis of the maser feature distribution. An edge-on rotating disk interpretation appears to be less probable, since the disk radius and the line-of-sight velocity dispersion as deduced by the observed H₂O maser distribution would imply an enclosed mass of only $\approx 1 M_{\odot}$; this would be in conflict with the (IRAS) bolometric luminosity, which indicates the presence of an intermediate- or high-mass YSO ($M \geq 6 M_{\odot}$).

On the contrary, towards Sh 2-255 IR, all the measured *relative* proper motions are approximately perpendicular to the outflow axis. In order to obtain for all the maser features absolute velocities directed along the large scale molecular outflow axis, the reference maser feature should move significantly faster ($\geq 100 \text{ km s}^{-1}$) than the measured relative proper motions. The best fit solution (found including line-of-sight and transversal velocities) for the conical outflow has a large opening angle, with the cone axis nearly perpendicular to the line-of-sight. The orientation of the fitted cone axis onto the plane of the sky is quite different from that of the large scale “Br γ /H₂ jet”. Differences in orientation between the outflow structures on large ($> 10000 \text{ AU}$) and small ($\leq 500 \text{ AU}$) scales might be due to either density gradients in the ambient medium, causing large-angle bends of the protostellar jets, or the presence of multiple, small-scale outflows, whose merging creates the large scale flow (Beuther et al. 2002a, 2003).

Towards IRAS 23139+5939, the CO outflow is nearly oriented along the line-of-sight and not spatially resolved on the plane of the sky. Since water maser features are seen projected onto the plane of the sky, the clustered distribution observed in this source (Fig. 2, lower panel) might result from a structure elongated along the line-of-sight, as it would be the case if maser emission were associated with the large-scale molecular outflow. This interpretation is consistent with the measured proper motions, suggestive of a general expansion. Accordingly, the best-fit conical solution has an axis oriented at close angle from the line-of-sight, with the vertex (YSO position) close to the geometrical centre of the circular cluster of features.

Towards WB89-234, all the measured proper motions have similar orientation, close to the direction of the molecular outflow, which might suggest that the measured, *relative*, transverse velocities represent well the “true” motion of the maser features, driven by the outflowing gas. The conical fit result supports these qualitative considerations, the axis of the best-fit cone having a projection onto the plane of the sky close to the position angle of the molecular outflow.

For IRAS 23139+5939 and WB89-234, a solution is found also for the Keplerian disk model but the fit of the measured velocities is worse than that for the outflow model. In addition, in both cases, the best solution has been found in correspondence of an edge-on disk, whose geometry is not supported by the observed spatial distribution of maser features that shows no preferential direction of elongation. The fitted disks have too large diameters ($\geq 10^4 \text{ AU}$) and are very poorly sampled by the detected maser features. In conclusion, we deduce that, towards both sources, a Keplerian disk interpretation is less likely than the proposed outflow model in accounting for the positions and velocities of the detected water maser features.

This analysis has revealed that the kinematics of water maser features observed towards Sh 2-255 IR, IRAS 23139+5939, and WB89-234 may be described by a conical outflow model. It is interesting to note that in each case (see Table 4) large opening angles of the conical jets are derived, supporting the case of large-angle winds. As outlined in Sect. 1, this result may be of particular interest to derive information on the evolutionary stage of a high-mass YSO and its consequences will be discussed in more detail in Sect. 4.3.

4.2. Physical environment of maser regions

Water masers are predicted to arise in the shocked layers of gas behind both high-velocity ($\geq 50 \text{ km s}^{-1}$) dissociative (J-type) (Elitzur et al. 1989) and slow ($\leq 50 \text{ km s}^{-1}$) non-dissociative (C-type) (Kaufman & Neufeld 1996) shocks, propagating in dense regions (pre-shock density $\geq 10^7 \text{ cm}^{-3}$).

If water masers originate in expanding jets (as suggested by the results discussed in the previous section), then the *absolute* velocity of a maser feature should indicate a lower limit for the shock velocity. In general, model fits reproduce the (well-measured) line-of-sight velocities better than the transversal ones, that are affected by larger errors. Then, to estimate the order of magnitude of absolute velocities on the plane of the sky, instead of using the values predicted by the models, for each component (along the RA and DEC axis) of the (relative) transversal velocity we have calculated the minimum and maximum variation from the mean value. The derived absolute velocities are found to be of the order of $8\text{--}21 \text{ km s}^{-1}$ (for Sh 2-255 IR), $26\text{--}103 \text{ km s}^{-1}$ (for IRAS 23139+5939) and $4\text{--}33 \text{ km s}^{-1}$ (for WB89-234). These velocities are much

Table 4: Best fit models results

Source name	α_c (")	δ_c (")	P_c (°)	i_c (°)	θ_c (°)	a_c (km s ⁻¹ arcsec ⁻¹)
Sh 2-255 IR	0.006	0.019	106	72	77	39
IRAS 23139+5939	0.025	0.025	264	23	78	320
WB89-234	0.003	-0.012	58	143	62	82

Note.— Col. 1 gives the source name, Cols. 2 and 3 report the (RA and DEC) sky-projected coordinates of the cone vertex, Cols. 4 and 5 the position angle and the inclination angle with the line-of-sight of the cone axis, Cols. 6 the opening angle of the cone, and Cols. 7 the velocity gradient.

larger than the sound speed ($v_s \leq 1$ km s⁻¹) of the dense ($n_{H_2} \geq 10^5$ cm⁻³) ambient medium through which the outflow is expected to propagate, so that shock waves appears as the natural explanation for the excitation of water masers. In particular, our results suggest that both C- and J-shocks could play a role in the excitation of water masers associated with jets, whereas the presence of extremely high velocity (> 100 km s⁻¹) shocks is not indicated by the velocity distribution of the observed water masers (varying in the range from ~ 1 to ~ 100 km s⁻¹ for the three sources).

Comparing the line-of-sight with the transversal velocities, one notes that for most of the maser features the relative transversal velocity is in general significantly larger than the corresponding line-of-sight velocity corrected for the molecular cloud LSR velocity. Interpreting maser features as shocks requires large differences in amplification gains along and across the direction of the shock motion. In particular, velocity gradients are likely to be the largest along the direction of motion, while the best velocity coherence with the longest gain paths should be encountered perpendicularly to the direction of motion (Elitzur et al. 1989). Since our EVN observations are sensitive only to the strongest features (≥ 0.4 Jy beam⁻¹), the observational result of transversal velocities larger than line-of-sight velocities might reflect the fact that we are observing preferentially shocks moving close to the plane of the sky.

Alternatively, if water masers originate on the surface of an accretion disk (as proposed for AFGL 5142-Group I, Paper I), they would feel the influence of the gravitational field of the massive YSO. At distances less than 10–15 AU from the high-mass YSO, models of accretion disks predict sufficiently high values of temperature (> 400 K) and density ($> 10^8$ cm⁻³) to match the physical conditions required for the excitation of the water masers. However, at larger distances, shock waves propagating through the disk might be required to warm and compress the maser gas. In this case, the pattern of Keplerian motion can be maintained as long as the shock velocity remains negligible compared to the Keplerian velocity. For the source AFGL 5142, the Keplerian disk model (which in this case also reproduces the transversal velocities well) gives absolute velocities of water masers in the range 7–32 km s⁻¹, corresponding to a range of disk radii from 1 to 400 AU. A

lower limit to the shock velocity can be estimated calculating the sound speed in an accretion disk around a massive YSO. The temperature as a function of the distance from the YSO can be estimated (in the hypothesis of heating by viscous dissipation) following the calculation by Natta (2000). The theoretical work by Palla & Stahler (1992) allows to estimate the mass and the radius of a massive proto-star (in this case, $15 M_\odot$ and $4.7 R_\odot$), assuming an accretion rate of $10^{-4} M_\odot$ yr⁻¹. The derived temperature of the disk varies from 20 to 1600 K when reducing the distance from the proto-star from 400 to 1 AU, respectively. This temperature range translates into a variation of the sound speed within the range 0.3–2.4 km s⁻¹. This indicates that, if moderate velocity shocks (Mach number ≤ 10) propagating throughout the disk are responsible for the maser excitation, the pattern of Keplerian velocities can be maintained.

Towards each of the observed sources (with the exception of WB89-234), a radio continuum source is detected. Traditionally, the detection of a radio continuum source has been taken as a proof of the ignition of the nuclear H burning reactions in the nucleus of the forming star: the heated photosphere would supply the UV radiation field needed to create an ionized envelope, which consequently would emit free-free radiation at radio frequencies. However, since the water maser emission is likely excited by shock waves, the shocks themselves might also account for the radio continuum emission detected towards the YSOs. In this interpretation, the free-free emission would be produced by the shocked, collisionally ionized gas.

Following the theoretical work of Ghavamian & Hartigan (1998), assuming a pre-shock density greater than 10^7 cm⁻³ (as suggested by the model of Elitzur et al. 1989) and a shock velocity in the range 5–100 km s⁻¹ (as estimated in the previous analysis), one would estimate an expected radio flux density of the order of 1 mJy, which agrees with the fluxes observed towards our sources. At the same time, this model allows to constrain the pre-shock density, shock velocity, and viewing angle to the source knowing the (resolved) angular size, flux density, and spectral index of a thermal radio source (at frequencies of 1.5, 5, and 15 GHz). Among the studied YSOs, an estimate of the spectral index α of the radio continuum source (defined as $S_\nu \propto \nu^\alpha$) is available only

for AFGL 5142 (observed at 5 GHz by McCutcheon et al. 1991; flux ≈ 0.5 mJy, spectral index ≈ 0.6) and OMC2 (observed at 15 GHz by Rengarajan & Ho 1996; flux ≈ 2.5 mJy, spectral index ≈ 0.44). Using these values, free-free emission of the order of 1 mJy is accounted for, with densities and shock velocities of 10^7 – 10^8 cm $^{-3}$ and ≤ 100 km s $^{-1}$, respectively. These values are in agreement with the densities required by maser excitation models (Elitzur et al. 1989; Kaufman & Neufeld 1996) and with the measured (and modeled) velocities.

4.3. Which evolutionary stage(s) trace water masers?

The standard theory of star formation predicts the formation of an accretion disk, as a consequence of the conservation of the angular momentum of the progenitor molecular cloud. During the accretion phase, the infalling matter suppresses any incipient stellar wind. Breakout will occur through the channel of weakest resistance, and as long as the gas continues to fall onto the disk rather than directly onto the star, this will be at the rotational poles of the accreting protostar, resulting in the ejection of a bipolar jet, *collimated* along the disk axis. It is plausible that the opening angle of the bipolar outflow widens with time and becomes nearly isotropic, since the wind gradually feels less resistance as the circumstellar envelope disappears. Following this “standard” paradigm, the occurrence of wide-angle conical jets, such as those proposed to explain the water maser kinematics in the studied YSOs, would indicate an evolved phase of the YSO.

Torrelles et al. (2003) proposed a different scenario, where *non-collimated* outflows may result from the emission of wide-angle winds by the YSO at the beginning of its evolution. Subsequently, the initially isotropic stellar wind may be channelled into a bipolar form by an anisotropic distribution of matter in the surrounding circumstellar environment, originating the collimated outflows commonly observed on large scales towards SFRs. Following this alternative scenario, the observed YSOs could be in a very early evolutionary stage (possibly in a proto-stellar phase).

In order to discriminate between these alternative schemes, we have tried to derive further information on the evolutionary stages of the studied YSOs based on the radio, millimeter and infrared continuum emissions.

As pointed out in the previous section, the assumption of ionizing flux from the YSO is not absolutely necessary to explain the observed radio continuum emission: it might in principle occur during the proto-stellar phase, excited by shocks associated to the accretion process and/or induced by stellar winds. On the other hand, accretion rates as high as 10^{-3} M $_{\odot}$ yr $^{-1}$ are expected to occur in massive YSOs (Osorio et al. 1999; Beuther et al. 2002b) and such massive infalls could cause the quenching of the UCHII radio emission, preventing its detection even if the YSO is already on the ZAMS (see e.g. Palla & Zinnecker 2002). Hence, the presence or the lack of radio continuum

emission furnishes no indication to distinguish between the proto-stellar and the ZAMS phase.

For low-mass stars, AWB suggested an empirical evolutionary classification, based on the ratio between the bolometric luminosity, L_{bol} , and the monochromatic luminosity at 1.3 mm, L_{mm} . Since in the proto-stellar phase the bolometric luminosity is a rising function of the stellar mass, while the luminosity at 1.3 mm is proportional to the mass of the accreting envelope, the ratio $L_{\text{bol}}/L_{\text{mm}}$ is thought to provide a relative measure of the mass ratio M_{*}/M_{env} : in this scheme, sources with lower values of this ratio are less evolved. For example, true protostars (the so called Class 0 objects) should have $M_{*}/M_{\text{env}} < 1$, corresponding to $L_{\text{bol}}/L_{\text{mm}} \leq 2 \times 10^4$ (AWB).

Despite bolometric and millimeter luminosities for all our sources but WB89-234 are available in literature, we believe that the same technique, applied successfully to low-mass-mass YSOs, cannot be applied to their high-mass counterparts, and hence, to our studied objects. In principle, one could calculate the $L_{\text{bol}}/L_{\text{mm}}$ ratio and derive a tentative evolutionary pattern for our high-mass YSOs to determine if they are in a protostellar or ZAMS phase. However, the basic assumption made by AWB that $L_{\text{bol}} \propto M_{*}$ (i.e. that the object luminosity derives only from the conversion of its gravitational energy) is valid only if we are dealing with “true” protostellar objects, that is precisely the information we are seeking for. For a ZAMS star the mass-luminosity relation would be totally different rendering the method by AWB not applicable.

Even if sensitive and high resolution observations of a high-mass YSO were available providing accurate values of its radio, millimeter, and infrared luminosities (allowing to disentangle its emission from contributions of other closeby YSOs), these data alone would not suffice to establish its evolutionary stage. A possible way to face the problem is complementing the continuum data with high-angular resolution, thermal or maser line observations, in order to derive information on the kinematics of the gas close to the YSO. In the case that the measured pattern of motion were compatible with rotation and/or contraction in a keplerian disk, one might derive the dynamical mass of the central object, M_{*} . Then, using the accreting envelope mass, M_{env} , estimable through millimeter continuum data, one might calculate the M_{*}/M_{env} ratio, which would provide a direct information on the evolutionary stage of the YSO.

5. Conclusions

Using the EVN we have conducted VLBI observations of the 22.2 GHz water masers towards four high-mass SFRs (Sh 2-255 IR, IRAS 23139+5939, WB89-234, OMC2) for three epochs (from June to November 1997). The water maser emission likely originates close (within hundreds of AU) to a forming high-mass YSO. Several distinct maser features (on average ≈ 10) have been detected for each source and, for those persistent over three epochs, proper motions are derived. The amplitudes of the proper mo-

tions are generally found to be larger than the range of variation of the corresponding line-of-sight velocities. For each source, the proper motion orientation is indicative of expansion. The LSR velocity variation of water maser features agrees with the line-of-sight velocity dispersion of the molecular outflows detected towards the four high-mass YSOs.

Three different kinematic models, i.e. a spherical expanding shell, a Keplerian rotating disk, and a conical outflow have been fitted to the 3-dimensional velocity field of the detected maser features. The results of the model fits suggest that the water maser features are most likely tracing the inner portion of the molecular outflows detected at much larger scales. In each case large opening angles of the conical jets are derived.

The gas kinematics as traced by the observed water masers is compatible with the prediction that in star-forming regions the 22.2 GHz H₂O masers arise behind shock waves. The shocks themselves may also account for the excitation of the radio continuum sources detected towards 3 out of 4 of the studied high-mass YSOs.

Basing on current theories of star formation and recent observational evidences of outflow collimation, we believe that the wide-angles derived for the conical-jets in our YSOs indicate a particular evolutionary stage, either evolved or extremely young. However, from the data available at present it is impossible to confidently discriminate between the two scenarios and trace an evolutionary pattern for our high-mass YSOs.

The fact that only 5-6 antennas could take part in each of our EVN observations is reflected in a limited channel map sensitivity threshold (≈ 0.3 Jy/chan). Hence, we are planning to carry out higher-sensitivity multi-epoch VLBA observations of this sample of YSOs, in order to better constrain the kinematic scenario suggested by this work.

Acknowledgements. The European VLBI Network is a joint facility of European, Chinese, South African and other radio astronomy institutes funded by their national research councils.

We are very grateful to R. Cesaroni for providing the VLA map of 22.2 GHz H₂O masers for the source Sh 2-255 IR.

References

André, P., Ward-Thompson, D., & Barsony, M. 1993, ApJ, 406, 122

Aso, Y., Tatematsu, K., Sekimoto, Y., et al. 2000, ApJS, 131, 465

Beuther, H., Schilke, P., Gueth, F., et al. 2002a, A&A, 387, 931

Beuther, H., Schilke, P., Sridharan, T. K., et al. 2002b, A&A, 383, 892

Beuther, H., Schilke, P., & Stanke, T. 2003, A&A, 408, 601

Beuther, H., Walsh, A., Schilke, P., et al. 2002c, A&A, 390, 289

Brand, J. & Wouterloot, J. G. A. 1998, A&A, 337, 539

Chini, R., Reipurth, B., Ward-Thompson, D., et al. 1997, ApJ, 474, L135

Claussen, M. J., Marvel, K. B., Wootten, A., & Wilking, B. A. 1998, ApJ, 507, L79

Elitzur, M., Hollenbach, D. J., & McKee, C. F. 1989, ApJ, 346, 983

Evans, N. J., Beckwith, S., & Blair, G. N. 1977, ApJ, 217, 448

Fischer, J., Sanders, D. B., Simon, M., & Solomon, P. M. 1985, ApJ, 293, 508

Genzel, R. & Downes, D. 1979, A&A, 72, 234

Ghavamian, P. & Hartigan, P. 1998, ApJ, 501, 687

Goddi, C., Moscadelli, L., Alef, W., & Brand, J. 2004, A&A, 420, 929

Howard, E. M., Pipher, J. L., & Forrest, W. J. 1997, ApJ, 481, 327

Imai, H., Kameya, O., Sasao, T., et al. 2000, ApJ, 538, 751

Jones, T. J., Mergen, J., Odewahn, S., et al. 1994, AJ, 107, 2120

Kaufman, M. J. & Neufeld, D. A. 1996, ApJ, 456, 250

McCutcheon, W. H., Sato, T., Dewdney, P. E., & Purton, C. R. 1991, AJ, 101, 1435

Mezger, P. G., Chini, R., Kreysa, E., Wink, J. E., & Salter, C. J. 1988, A&A, 191, 44

Mezger, P. G., Zylka, R., & Wink, J. E. 1990, A&A, 228, 95

Miralles, M. P., Salas, L., Cruz-Gonzalez, I., & Kurtz, S. 1997, ApJ, 488, 749

Moscadelli, L., Cesaroni, R., & Rioja, M. J. 2000, A&A, 360, 663

Natta, A. 2000, in *Infrared Space Astronomy, Today and Tomorrow*, 193

Osorio, M., Lizano, S., & D'Alessio, P. 1999, ApJ, 525, 808

Palla, F. & Stahler, S. W. 1992, ApJ, 392, 667

Palla, F. & Zinnecker, H. 2002, *Physics of Star Formation in Galaxies, Saas-Fee Advanced Course 29, Les Diablerets, Switzerland, 22 to 29 March 1999*, ed. A. Maeder & G. Meynet (Berlin: Springer Verlag), 1–133

Panagia, N. 1973, AJ, 78, 929

Pendleton, Y., Werner, M. W., Capps, R., & Lester, D. 1986, ApJ, 311, 360

Reipurth, B., Rodríguez, L. F., & Chini, R. 1999, AJ, 118, 983

Rengarajan, T. N. & Ho, P. T. P. 1996, ApJ, 465, 363

Seth, A., Greenhill, L. J., & Holder, B. P. 2002, ApJ, 581, 325

Snell, R. L. & Bally, J. 1986, ApJ, 303, 683

Sridharan, T. K., Beuther, H., Schilke, P., Menten, K. M., & Wyrowski, F. 2002, ApJ, 566, 931

Tofani, G., Felli, M., Taylor, G. B., & Hunter, T. R. 1995, A&AS, 112, 299

Torrelles, J. M., Gomez, J. F., Rodriguez, L. F., et al. 1996, ApJ, 457, L107

—. 1997, ApJ, 489, 744

Torrelles, J. M., Patel, N. A., Anglada, G., et al. 2003,
ApJ, 598, L115

Torrelles, J. M., Patel, N. A., Gómez, J. F., et al. 2001,
Nature, 411, 277

Wouterloot, J. G. A. & Brand, J. 1989, A&AS, 80, 149

Wouterloot, J. G. A., Henkel, C., & Walmsley, C. M. 1989,
A&A, 215, 131

Yu, K., Bally, J., & Devine, D. 1997, ApJ, 485, L45

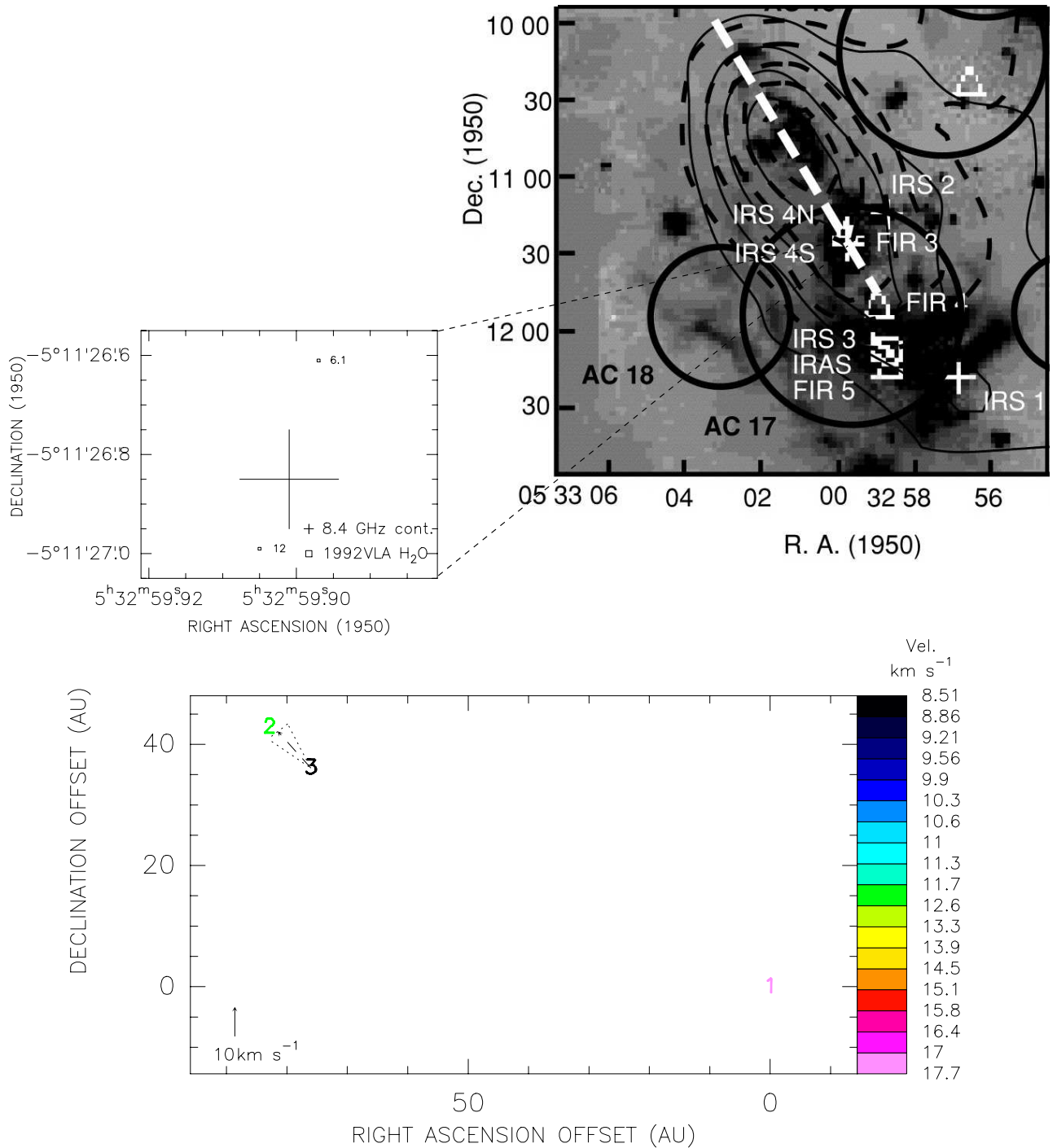


Fig. 4. OMC2. (Upper panel) Blue wings (solid lines) and red wings (dashed lines) in the HCO^+ line tracing the outflow (Aso et al. 2000), superimposed on the image of H_2 emission (grey scale) (Yu et al. 1997); the white dashed-line indicates the elongation axis of the outflow; the positions of IRS4 and FIR 3 are also shown. (Middle panel) Positions (open squares) and the LSR velocities of 22 GHz H_2O maser features detected with the VLA in 1992 by Tofani et al. (1995); the cross indicates the positional uncertainty of the 8.4 GHz continuum source. (Bottom panel) VLBI map of the 22.2 GHz water maser features (see the caption of Fig. 1), with positions relative to the reference feature “1”.